Sedimentation-Based Confinement of Individual Giant Unilamellar Vesicles in Microchamber Arrays with a Dynamically Exchangeable Outer Medium

Syed Kaabir Ali, Catherine Sella, Vadim Dilhas, Barbara Jacková, Marina Mariconti, Clara Gomez-Cruz, Laurent Thouin, Mathieu Morel, Damien Baigl, Ayako Yamada

Sedimentation-based Confinement of Individual Giant Unilamellar Vesicles in Microchamber Arrays with a Dynamically Exchangeable Outer Medium

Syed Kaabir Ali[1], Catherine Sella[1], Vadim Dilhas[1], Barbara Jacková[1], Marina Mariconti[1], Clara Gomez-Cruz[1], Laurent Thouin[1], Mathieu Morel[1], Damien Baigl[1], and Ayako Yamada[1]*

[1] *PASTEUR, Department of Chemistry, Ecole Normale Supérieure, PSL University, Sorbonne Université, CNRS, 75005 Paris, France*

* Correspondence to: ayako.yamada@ens.psl.eu

Abstract

Giant unilamellar vesicles (GUVs) are an ideal model to study cellular membrane functions *in vitro*, yet difficult to manipulate due to their fragile nature, especially when subjected to dynamic change of their external microenvironment. Here, an original microfluidic concept is introduced for constraint-free confinement of individual GUVs in microchambers with a dynamically exchangeable outer medium. GUVs self-confine in an array of laterally separated microchambers by sedimentation, avoiding any mechanical constraint while allowing diffusion-based exchange of the outer medium via a microfluidic channel and time-resolved microscopy observation. The geometric and flow parameters optimizing medium exchange while preventing GUV from lifting out are numerically established. Different aqueous solutions separated by air plugs can be flowed into the channel by taking advantage of a polydimethylsiloxane-based hydrophilic channel wall. The possibility to manipulate microliter sample volumes for in situ observation of protein cell-free expression is also exploited. It is found that the membrane-targeting sequence of Bacillus subtilis MinD binds to GUVs and induces extensive membrane tubulation. This technically simple method offers a robust way to confine GUVs and dynamically control their outer medium, thus constituting an ideal platform to study the spatio-temporal response of reconstituted membranes and/or synthetic cell studies subjected to dynamic micro-environments.

1. Introduction

Giant unilamellar vesicle (GUV), a cell-sized closed phospholipid bilayer membrane, has been extensively exploited as both synthetic cells and *in vitro* models of cell and cell organelle membranes [1–4]. GUVs are manipulable individually by micropipette under precise control of membrane tension, which enables, for example, characterizing physicochemical properties of the membrane via submicron-diameter membrane tubes pulled out from a GUV for several tens of microns [5–7]. Their deformability, in turn, makes them difficult to handle in a high throughput manner, in particular, with changes of their environment. In this context, microfluidics technology has been employed to capture a large number of GUVs using microstructures [8–12]. For instance, an elaborate system has been developed by T. Robinson, *et al*. [8] where individual GUVs were captured hydrodynamically in a micropocket [13] inside an isolating chamber, which can be opened and closed for medium exchange. The hydrodynamic traps were combined in the work of Y. Kazayama *et al*. with deterministic lateral displacement [14] for a high selectivity of trapped GUVs [9]. In both cases, GUVs are in

contact with the micropocket walls, which in some cases can be an obstacle to assess the behavior of a free GUV membrane. Besides, delicate control of flows is required to keep the hydrodynamic trapping. Interestingly, K. A. Ganzinger *et al*. took advantage of the mechanical constraint of the micropockets to strongly deform GUVs [10]. The common point in all these works is a necessary mechanical constraint by solid walls on the GUVs and limited external medium exchange possibilities, resulting in efficient trapping yet difficulty to study the behavior of free, unconstrained membranes, especially in a dynamic microenvironment. We reported an alternative where microwells etched on the ceiling of a microfluidic channel were used to trap and release GUVs by elastic energy gradient [11]. In this configuration, free GUV membranes can be assessed while being trapped. However, the system is sensitive to the membrane tension of GUVs and thus not suitable for assays accompanied by GUV deflation. In contrast with the above mentioned devices that aim at trapping single GUVs, N. Yandrapalli, *et al*. proposed a strategy to confine large assemblies of GUVs in cages of micropillars with the possibility of solution exchanges [12]. While this device allows the observation of a large number of GUVs at once, GUVs are highly packed in the cage resulting in highly constrained membranes.

Herein, we introduce a microfluidic concept, in which a large number of individual GUVs self-confine by sedimentation in microwells covered with channels allowing exchanges of their outer medium. The thin bottom layer of the microwells allows dynamic microscopy observations of GUVs, with no contact with the lateral walls and free from mechanical constraint, at a high magnification. A water reservoir placed closely above the channels prevents evaporation through the channel wall during hours, allowing long-term biochemical reactions such as gene expression at 37 °C [15].

Microwells have been widely used to capture single cells for more than a decade [16, 17] besides other microfluidic techniques developed for cell or particle trapping [18]. Owing to the higher density compared to GUVs and the monodispersity of cells, microwells can achieve a remarkably high cell trapping efficiency [16, 17]. Microwells can also be used to form and culture micro-tissues such as spheroids [19], or to reconstitute cellular architecture *in vitro* [20, 21]. Overall, despite their broad demonstrated applicability for cell or particle trapping and exchange medium capability, to our knowledge, there is no demonstrated example of efficient GUV trapping in microwell arrays. Moreover, various materials, such as polydimethylsiloxane (PDMS), polystyrene, hydrogels, or UV-curable resins have been used for microwells and we feel it is also interesting to explore alternative materials that could combine easy fabrication

and good optical performance for microscopy characterization. In this study, we thus not only propose a concept ofmicrowell array allowing efficient GUV trapping but also establish a simpler fabrication protocol involving a photoresist that was not explored so far and that is advantageously devoid of any autofluorescence emission, both under visible and UV light excitation.

To enable sequential exchanges of the outer medium of GUVs in a small volume, while keeping the device immobile on a microscopy stage, air plugs can be used to separate different solutions in single tubing connected to a pump [22, 23]. However, due to the hydrophobic nature of conventional microfluidic channel surfaces, e.g. PDMS, introduction of air in a channel is usually undesired since it leaves air bubbles pinned at the channel surface. A smart solution to turn PDMS into a hydrophilic surface has been proposed recently by Gokaltun, *et al*., and consisted in adding a block copolymer of dimethylsiloxane and ethylene oxide to PDMS [24]. By combining those methodologies, we demonstrate that the outer medium of GUVs can be exchanged multiple times in our device under microscopy observation. Moreover, a volume of the outer medium as small as 10 μL being required, the device is advantageous for biochemical assays targeting model membranes with precious reagents. During the medium exchange, however, GUVs tend to escape from shallow microwells due to a lift force induced by the medium flow above the microwells. To find an optimal range of well depth and flow velocity, numerical simulations have been performed following the strategy used in the study on spheroid trapping in microwells by Rousset, *et al*. [25]

Lastly, the applicability of our device to in situ biochemical reactions in the presence of GUVs is investigated. As a proof of concept, a cell-free gene expression has been performed, which is challenging because of the high osmolality of the medium and hours of incubation process at 37 °C. A membrane-targeting sequence of Bacillus subtilis MinD, bsMTS, is expressed using the cell-free system in the presence of GUVs and is allowed to interact with their membrane. We demonstrate that YFP-conjugated bsMTS is successfully expressed in the device in the presence of GUVs and binds to the bilayer membrane containing a negatively charged lipid. Moreover, spontaneous membrane tubulation from the GUVs occurs upon the expression of YFP-bsMTS.

2. Results and Discussion

2.1. Microfluidic Device Characterization

As illustrated in Figure 1a, a thin photoresist layer with microwells was covered by a PDMS layer containing a microfluidic circuit consisting here in two parallel straight channels. To avoid evaporation through PDMS, a water reservoir was added in the vicinity of the channels, covering most of the channel areas except their extremities [15]. A photograph of the assembled microfluidic device is shown in Figure 1b. The microwells had a diameter of 40 μm and were distributed at 40 μm intervals, covering an area of 15 mm × 25 mm as illustrated in Figure S1a (Supporting Information). The two channels were designed to have a width and a length of 3 mm and 2 cm, respectively, smoothly connected to their inlets and outlets as depicted in Figure S1b (Supporting Information). Each channel covered *ca.* 1.1×10^4 microwells. The final depths of the microwells were smaller than the thickness of the original photoresist dry films used for a master mold fabrication due to compression during dry film lamination and PDMS mold replication processes: the wells fabricated with 50- and 100 μm-thick films had a depth of 43.0 ± 0.2 and 91.5 ± 0.1 μm, respectively. The channels fabricated from 50- and 100 μm-thick films had a final height of 46.3 ± 0.4 and 100.7 ± 3.2 μm, respectively, corresponding to channel volume of 3.1 and 6.8 μL, respectively. As described in Supporting Information, microwells were fabricated in OrmoStamp photoresist by soft lithography directly on a thin cover glass slide. Although a thin layer of the photoresist was remaining at the bottom of the microwells, its thickness, 6.5 ± 5.2 μm, was small enough to allow high-magnification microscopy observations of GUVs inside the microwells. It is worth noting that the microwell layer can be fabricated rapidly in less than 20 min once a PDMS mold is obtained, and that OrmoStamp was selected as the material for the microwells among other UV-sensitive resins because of its low autofluorescence both under visible and UV light excitation.

2.2. GUV Trapping

GUVs formed by electroformation [26, 27] in a sucrose solution were introduced in the microfluidic device and let to sediment in a 1:1 (v/v) mixture of sucrose and glucose solution at the same osmolality. To avoid the bursting of GUVs, the channel and microwell surfaces were coated with 0.5% (w/v) β-casein or 5% (w/v) bovine serum albumin in phosphate-buffered saline (PBS), and the osmolalities of the sucrose solution and the outer medium were carefully adjusted as described in Supporting Information. Due to the density difference, GUVs sedimented at the bottom of the channel, and some of them further fell into the microwells, leading to spontaneous GUV confinement in laterally isolated microchambers with an open ceiling for medium exchange. The GUVs that remained outside the wells were carried away upon fluid exchange as depicted in Figure 1c. Figure 1d and Figure S2 (Supporting

Information) show a representative images of GUVs composed of L-α-phosphatidylcholine from chicken egg (EPC) and a fluorescent lipid, Texas Red 1,2-dihexadecanoyl-snglycero-3-phosphoethanolamine (Texas Red DHPE), trapped in the microwells after the channel was rinsed with a solution without GUV. It shows that, after their sedimentation in the wells, the GUVs remained confined during the medium replacement in the upper microfluidic channels. To estimate the necessary time for GUVs to sediment in the microwells, an evaluation following an approximation made by Haberman *et al*. was employed [25, 28]. The terminal velocity U of a sphere with a radius r moving in a still medium in an infinite cylinder with a radius R can be described as

$$U = 2/9 \cdot r^2 g(\rho_o - \rho_i)(1+\sigma)/\mu K(1+2\sigma/3)$$

where g is gravitational constant, ρ_o and ρ_i are the densities of the outer and inner medium of the sphere, respectively, σ is the viscosity ratio of the outer to the inner medium, μ is dynamic viscosity of the outer medium, and K is a wall correction factor, which is a function of σ and $\delta = r/R$ [28]. Viscosities of 1:1 (v/v) mixture of sucrose and glucose solutions with an osmolality of 300 mOsm kg^{-1} H_2O used for most of the experiments and 1.72 Osm kg^{-1} H_2O used for the cell-free gene expression experiments were measured as 1.18 and 5.19 mPa s, respectively. The former was used for the following calculation together with ρ_o and ρ_i for 300 mOsm kg^{-1} H_2O mediums, 1.030 × 10^3 kg m^{-3} and 1.037 × 10^3 kg m^{-3}, respectively. Although lipid bilayer membranes in disordered phases are fluidic with certain viscosities [29–33], when a GUV sediments vertically, there is no membrane flow due to the axial symmetry that prevents circulation of lipids in the membrane [34]. We thus assume $\sigma = 0$, which gives [28]

$$U = 2/9 \cdot r^2 g(\rho_o - \rho_i)/\mu K$$

and

$$K = (1 - 0.75857\delta^5)/(1 - 2.1050\delta + 2.0865\delta^3 - 1.7068\delta^5 + 0.72603\delta^6)$$

The graph in Figure 2a shows the value of U plotted against GUV diameter, $2r$, while the microwell diameter, $2R$, is fixed to 40 μm and $\mu = 1.2$ (magenta). For a comparison, the result when a GUV sediments in a still infinite medium, i.e. $K = 1$, is shown in green. In Figure 2b, the time necessary for a GUV to sediment for 40 μm in a 40 μm-diameter infinitely long cylinder, $T_{40\ \mu m}$, is plotted against GUV diameter in magenta, together with the case $K = 1$ in green. It shows that, for both configurations, all GUVs with a diameter larger than 2.2 μm sediment in less than 10 min (blue line). After introduction in a channel, GUVs were thus allowed to sediment for 10 min in a still medium, and this process was repeated twice. The size

distribution of GUVs right after the electroformation, with an average diameter of 4.4 ± 6.1 μm (n = 2984), is shown in magenta in Figure 3a. Interestingly, the peak of the size distribution of GUVs after trapping is shifted toward greater values as shown in yellow in Figure 3a, with an average diameter of 8.5 ± 5.6 μm (n = 1471). Due to a longer time necessary for small GUVs to sediment into microwells, GUVs with a diameter of a few μm can be excluded, in agreement with the result shown in Figure 2b, thus causing the shift. The number of GUVs with a diameter larger than 3 μm trapped per single microwell was also investigated. As shown in Figure 3b, a majority of the wells contained either 0 or 1 GUV. The distribution was reproducibly observed in 3 independent experiments and followed a Poisson distribution with as a mean number of GUV per well $\lambda = 0.40 \pm 0.16$, as indicated with black dots. The average GUV density of the solution introduced in the channel was $8.9 \pm 3.0 \cdot 10^3$ μL^{-1}. The number of trapped GUVs is affected by the initial GUV density since only GUVs positioned above microwell area can sediment into the microwells. Figure S3 in Supporting Information shows a fluorescence microscopy image of an initial GUV solution introduced in a 46.3 μm-high channel without microwells taken 10 min after the introduction (left), and a merged image of fluorescence and phase-contrast microscopy of the same solution after trapping operation, i.e., three times of 10 min GUV sedimentation and a rinse (right). The initial GUV density δ_{GUV} was measured using the channel without microwells, and the number of GUVs per microwell was counted after trapping GUVs from the same solution. Individual data of the three independent experiments can be found in Figure S4 in Supporting Information and show that λ increases with an increase in δ_{GUV} (Figure S5, Supporting information). Given the low density of GUVs, we assume that all the GUVs larger than 3 μm placed above a microwell sediment and become trapped in the microwell, without being repelled due to lack of space. Based on this assumption, the theoretical value of λ_{theo} taken as the average number of GUVs above each well after three fillings, can be written as $\lambda_{theo} = 3\delta_{GUV} \cdot H \cdot \pi R^2$ where H and R are the channel height and microwell radius, respectively. Although λ is systematically lower than λ_{theo}, probably due to some loss by GUV lifting (see below), we note that λ and λ_{theo} are of the same order of magnitude and follow the same δ_{GUV} dependence (Figure S5). This shows that, obeying a Poisson law the distribution at each filling step, the number of GUV can be predicted and controlled by adjusting the GUV density and the number of filling steps.

2.3. Molecular Diffusion in the Microwells Upon Medium Exchange

To estimate the necessary time to replace the medium in the microwells, we analyzed the molecular diffusion dynamics upon medium exchange in the absence of trapped GUVs. 10 μm

fluorescein in PBS was first introduced in a 46.3 μm-high channel, then PBS without fluorescein was subsequently flowed by a micro-peristaltic pump under microscopy observation. Figure 4a shows a series of fluorescence microscopy images taken at the edge (top) and center (bottom) of the channel at different time points. The flow velocity at the center of the channel induced by the peristaltic pump was measured as 6.49 ± 1.02 mm s^{-1} by tracking fluorescently labeled GUVs flowing in the channel in a separate experiment. Note that this flow velocity corresponds to *ca.* 0.90 μL s^{-1}, which is also comparable to gentle manual injection of medium to the device by micropipette. The fluorescence intensities in microwells at different positions were measured and plotted in Figure 4b for the microwells with two different depths. The distance between the microwell center and the channel edge is indicated with the color code on the right. The fluorescence decreases rapidly in particular at the channel center (black curves) as expected in a laminar flow due to a maximal linear flow velocity at the center of the channel. The results demonstrate that a few tens of seconds is enough to replace small molecules such as fluorescein in the microwells. The fluctuation in the curves is due to the fluctuation of flow velocity created by the peristaltic pump. Despite this issue, the peristaltic micro-pump is advantageous compared to a syringe pump or a pressure pump, since it can be directly placed on the microscopy stage closely connected to the device, and its flow rate as well as flow direction can be easily controlled, allowing us to control fluids swiftly without looking away from the device.

2.4. Sequential Medium Exchange with Air Plugs

Next, the possibility of sequentially introduce different mediums to the device with GUVs inside the microwells was investigated. To separate different solutions, ca. 10 μL air plugs were inserted between 10 μL of the solutions in a tubing connected to the peristaltic pump, as depicted in Figure 5a [22, 23]. Figure 5b shows the series of microscopy images taken at different steps, where different solutions were sequentially introduced into a 46.3 μm-high channel as follows. After GUV trapping, PBS (solution 1) was introduced in the channel as shown in the top left panel, where the fluorescence of GUVs composed of EPC and Texas Red DHPE is colored in red. Under microscopy observation, the solution was pushed throughout the channel by micropump, and replaced with air, leaving the solution 1 inside the microwells as shown in the upper, second left panel in Figure 5b. Subsequently, 10 μm fluorescein in PBS (solution 2), PBS (solution 3), and 10 μm fluorescein in PBS (solution 4) were introduced with air plugs in between. The fluorescence of fluorescein is shown in blue in Figure 5b. When the 43.0 μm-deep wells were used, a part of GUVs, in particular with a greater size, were lost

during this process as shown in Figure S6 (Supporting Information). This issue was overcome by increasing the well depth. As shown in Figure 5b, with 91.5 μm-deep microwells, the majority of GUVs remained trapped after the sequential medium exchanges as indicated with white arrowheads. Importantly, when pure PDMS was initially used for the device, some microwells were covered by air that remained in the channel due to the hydrophobic nature of PDMS and OrmoStamp. To avoid the air pinning, 0.25% (w/w) of dimethylsiloxane-(60–70% ethylene oxide) block copolymer (PDMS-EtO) was added to PDMS to turn the channel surface hydrophilic.[24] Therefore, with PDMS-EtO, the air plugs were smoothly moved throughout a 46.3 μm-high channel, without leaving air inside the channel as demonstrated in Figure 5c. This property was also significantly advantageous when the device was used manually without air plugs. The PDMS-EtO modification served as an effective preventive measure against the introduction of air bubbles. Furthermore, undesired air bubbles accidentally introduced in the device could be easily removed by flowing a solution with micropipette, in direct contrast to traditional PDMS featuring hydrophobic channel walls, where trapped air bubbles could potentially inflict damage on the sample and/or alter the fluid flow.

2.5. Numerical Simulations of Molecular Diffusion and the Lift Force on GUVs in the Microwells

Next, we evaluated molecular diffusion upon medium exchange as well as the lift force that made GUVs escape from the microwells in silico using COMSOL Multiphysics 6.0 software. As depicted in Figure S7 (Supporting Information), the 3D geometry of the model included 9 microwells with a depth h and a diameter of 40 μm were positioned at a 40 μm interval at the bottom of a 300 μm-wide, 46.3 μm-high, and 400 μm-long channel geometry. To calculate the lift force on a GUV in a microwell, a solid sphere as amodel of a GUV with a diameter DGUV was positioned in the central microwell, at 1 μm distance from the microwell wall of the upstream side and of the bottom. The left panel in Figure 6a shows the evolution of average fluorescein concentration in a microwell with time, as a result of its diffusion from the well under a constant flow of medium without fluorescein introduced at the channel inlet at a velocity of 6.0 mm s^{-1}. The well depth was varied as indicated with a color code, while the viscosity μ of the medium was set as 1.0 mPa s. The curves for a depth of 43.0 (black) and 91.5 μm (red) correspond to the experimental conditions shown in the left and right panels of Figure 4b with black lines, respectively. Those curves and the experimental data are plotted on a same graph in Figure S8 (Supporting Information) for direct comparison. The experimental and simulation results give similar profiles and characteristic exchange times, validating the model

used for the simulations and confirming that fast-diffusing entities can be quickly exchanged in a few tens of seconds in the system. Another set of parameters was tested to simulate for a larger molecule in a viscous medium, as is the case for the cell-free gene expression experiment. For instance, a large protein involved in the early step of gene expression, T7 polymerase, is 99 kDa, and the viscosity of the sugar solution to reach the same osmolality as the cell-free system was 5.2 mPa s. As shown in the right panel in Figure 6a, a longer time is necessary for a large molecule in such a viscous medium to be carried away from the microwell with a large depth. Nonetheless, the required time falls in a range of a minute, which is negligible compared to characteristic times involved in gene expression. The micro-scale vertical confinement and the free diffusion allow a fast exchange of the outer medium of the confined GUVs, ranging from a few seconds for fast-diffusing molecules to a minute for large proteins. It is worth noting that there is a slow circulation inside the microwells as shown in Figure S9 (Supporting Information). Next, we established the conditions for which GUVs remained confined while subjected to a flow in the upper microfluidic channels. This was done by computing the lift force F_{lift} exerted on the GUVs by the flow and calculating the critical flow velocities, at which the lift force F_{lift} on a GUV equals the gravitational force $F_{\mathrm{g}} = 4\pi r^3 g(\rho_{\mathrm{i}} - \rho_{\mathrm{o}})/3$ [25]. Figure 6b shows the resulting phase diagram, in which each line depicts the critical flow velocity as a function of the GUV diameter and for different well depths. Below each line, the colored regions represent the parameter ranges suitable for GUV trapping under flow, i.e. $F_{\mathrm{lift}} \leq F_{\mathrm{g}}$. In a range of typical flow velocity made by the peristaltic micro-pump or by manual pipetting, i.e. up to several mm s−1, microwells with a depth of 70 μm or larger can trap GUVs at a high efficiency. This confirms the experimental results with 91.5 μm-deep wells shown in Figure 5b.

2.6. Cell-Free Gene Expression of Membrane Binding Protein in the Presence of GUVs

Finally, we characterized the applicability of this method for synthetic cell investigation, and in particular GUV exposure to biochemical reactions and in-situ response characterization. The system was applied in particular for in situ cell-free expression of a membrane-binding protein in the presence of GUVs trapped in the microwells and observation of the unconstrained membrane response. The cell-free gene expression system is composed of purified components necessary for the gene transcription and expression machinery of *Escherichia coli* [35, 36]. Here, fluid manipulations were done manually by micropipette, which took *ca.* 15–20 s for each fluid injection. Since the cell-free gene expression system is sensitive to dilution, a combination of a larger channel height (100.7 ± 3.2 μm) and smaller well depth (43.0 ± 0.2

μm) was exploited for a better fluid exchange inside microwells, even though the GUV trapping efficiency is lower with shallow wells as shown in Figure 6a (right) and Figure 6b. GUVs were composed of a 4:1 (mol mol−1) mixture of 1,2-dioleoyl-snglycero-3-phosphocholine (DOPC) and a negatively charged lipid, 1,2-dioleoyl-sn-glycero-3-phospho-(1'-rac-glycerol) (DOPG), with a small fraction of Texas Red DHPE. After GUV sedimentation, the solution in one channel was replaced with a cell-free gene expression medium containing a plasmid DNA, nucleotides, amino acids, and proteins necessary for transcription and translation machinery, as well as chaperons and disulfide bond enhancers as illustrated in Figure 7a and detailed in Supporting Information. The same medium without plasmid DNA was introduced in the other channel. The plasmid DNA was coding for a membrane targeting sequence (MTS) of *Bacillus subtilis* MinD fused at C-terminus with PhiYFP (YFP-bsMTS), as its amino acid sequence depicted in Figure 7b. After the introduction of the cell-free expression medium, the entire chip was incubated at 37 °C in a humidified chamber for 3.5 h before confocal microscopy observation. The fluorescence of the GUV membrane and YFP-bsMTS were observed with excitation wavelengths at 543 and 488 nm, and emission wavelengths at 599–797 and 518–571 nm, respectively. Surprisingly, a significant number of membrane tubes were formed from single GUVs as shown in Figure 7c, whereas in the control channel without plasmid DNA, GUVs kept their spherical shape after 3.5 h incubation at 37 °C as shown in Figure 7d. Significant numbers of membrane tubes were observed on 91 ± 4% of GUVs in microwells at different areas in the channel (3 independent experiments, n = 13, 20, 20). As a comparison, we have performed YFP-bsMTS expression in the presence of GUVs without trapping, at different volume fractions of GUV solution in the cell-free expression medium. As shown in Figure S10 (Supporting Information), we have observed a heterogeneous population of GUVs interacting differently with the protein, and membrane tube formation was observed on 44 ± 11% of GUVs only. In the bulk experiment, the more GUVs are added, the more their outer medium becomes diluted, leading to a less efficient protein expression. Moreover, the sample solution cannot be rigorously mixed due to the fragility of GUVs, which may lead to a heterogeneous reaction in the bulk experiment. It is worth noting that membrane tubes were not spread in a large distance as observed in microwells, probably due to the shear the GUVs experienced during the transfer to the observation chamber and sedimentation in the chamber for a millimetric distance. Those observations clearly show that not only our system allows to observe dynamic membrane response with minimal perturbation (no constraint on the membrane) but also demonstrates several advantages over a bulk experiment such as higher

control (and purity) of the outer medium, better reproducibility and less mechanical perturbations. We also confirmed that in the absence of the negatively charged DOPG, YFP-bsMTS did not bind to the GUV membrane, leaving the GUVs unchanged (data not shown). MinD, together with MinC, is a key player in the positioning of division protein at mid-cell in *B. subtilis* [37]. It has been shown that negatively charged lipid is enriched in a spiral shape along the longitudinal axis of the bacteria and MinD colocalizes with the lipid spiral via its bsMTS that is in a shape of α-helix [38]. However, bsMTS or MinD has never been shown to create or favor a positive membrane curvature. Spontaneous membrane tubulation from GUVs have been observed in different contexts, caused by a local charge gradient [39–41], anchoring of amphiphilic molecules [42], transbilayer charged lipid asymmetry [43], or by asymmetric binding of proteins [44, 45]. Interestingly, Stachowiak *et al*. demonstrated that even proteins unrelated to membrane curvature can drive membrane tubulation by protein-protein crowding [45]. Our case, yet to be investigated further, may fit in this criterion.

3. Conclusion

We have developed a microfluidic device, with a reasonably quick fabrication protocol and of easy handling, to capture GUVs by spontaneous sedimentation into microwells at the bottom of microfluidic channels, covered with a water reservoir to avoid evaporation through the channel wall. The device allows time resolved, high-magnification observation of GUVs under dynamic medium changes while avoiding the mechanical constraints usually necessary in conventional trapping approach. The device is compatible with fluorescence microscopy observation with an excitation at UV or visible wavelength. Optimal conditions of well depths and flow velocity were searched in silico, supporting our experimental results, and allow designing devices where GUVs outer medium can be changed in minute time scale. In situ cell-free gene expression of a membrane binding protein in the presence of GUVs was successfully performed in the device, which led to membrane tubulation from the GUVs, demonstrating advantages over bulk manipulations for reproducible observation of unconstrained membrane dynamic behavior under a changing external micro-environment. Easy to use and to adapt for optimal performance, the device applies to a wide range of biochemical and biophysical assays using GUVs as a model membrane, as well as targeting other microscale objects such as colloid particles, single cells, and purified cell organelles [46–49].

Acknowledgements

This work was supported by the French National Research Agency ANR through contracts Single Nuclei on Chip via Institut Pierre-Gilles de Gennes (IPGG), Brain-hive via Institut Carnot IPGG (laboratoire d'excellence, Investissements d'avenir program ANR-10-IDEX-0001-02 PSL, ANR-10-LABX-31), and SCDiag (ANR-21-CE18-0051). This work has benefited from the technical contribution of the joint service unit CNRS UAR 3750 (IPGG). The authors thank Drs. Nathalie Delgehyr (Institut de Biologie de l'Ecole Normale Supérieure), Julie Plastino, Christine Gourier (Laboratoire de Physique de l'Ecole normale supérieure), and Saikat Saha (Department of Chemistry, Ecole Normale Supérieure) for fruitful discussions.

References

[1] A. Roux, G. Cappello, J. Cartaud, J. Prost, B. Goud, P. Bassereau, *Proc. Natl. Acad. Sci.* **2002**, *99*, 5394.

[2] W. Romer, L. Berland, V. Chambon, K. Gaus, B. Windschiegl, D. Tenza, M. R. E. Aly, V. Fraisier, J. C. Florent, D. Perrais, C. Lamaze, G. Raposo, C. Steinem, P. Sens, P. Bassereau, L. Johannes, *Nature* **2007**, *450*, 670.

[3] A. Yamada, A. Mamane, J. Lee-Tin-Wah, A. Di Cicco, C. Prevost, D. Levy, J. F. Joanny, E. Coudrier, P. Bassereau, *Nat. Commun.* **2014**, *5*, 3624.

[4] C. Simon, R. Kusters, V. Caorsi, A. Allard, M. Abou-Ghali, J. Manzi, A. Di Cicco, D. Levy, M. Lenz, J. F. Joanny, C. Campillo, J. Plastino, P. Sens, C. Sykes, *Nat. Phys.* **2019**, *15*, 602.

[5] D. Cuvelier, I. Derenyi, P. Bassereau, P. Nassoy, *Biophys. J.* **2005**, *88*, 2714.

[6] S. Morlot, V. Galli, M. Klein, N. Chiaruttini, J. Manzi, F. Humbert, L. Dinis, M. Lenz, G. Cappello, A. Roux, *Cell* **2012**, *151*, 619.

[7] S. Aimon, A. Callan-Jones, A. Berthaud, M. Pinot, G. E. S. Toombes, P. Bassereau, *Dev. Cell* **2014**, *28*, 212.

[8] T. Robinson, P. Kuhn, K. Eyer, P. S. Dittrich, *Biomicrofluidics* **2013**, *7*, 44105.

[9] Y. Kazayama, T. Teshima, T. Osaki, S. Takeuchi, T. Toyota, *Anal. Chem.* **2016**, *88*, 1111.

[10] K. A. Ganzinger, A. Merino-Salomon, D. A. Garcia-Soriano, A. N. Butterfield, T. Litschel, F. Siedler, P. Schwille, *Angew. Chem. Int. Ed. Engl.* **2020**, *59*, 21372.

[11] A. Yamada, S. Lee, P. Bassereau, C. N. Baroud, *Soft Matter* **2014**, *10*, 5878.

[12] N. Yandrapalli, T. Robinson, *Lab Chip* **2019**, *19*, 626.

[13] D. Di Carlo, N. Aghdam, L. P. Lee, *Anal. Chem.* **2006**, *78*, 4925.

[14] L. R. Huang, E. C. Cox, R. H. Austin, J. C. Sturm, *Science* **2004**, *304*, 987.

[15] A. Yamada, F. Barbaud, L. Cinque, L. Wang, Q. A. Zeng, Y. Chen, D. Baigl, *Small* **2010**, *6*, 2169.

[16] J. R. Rettig, A. Folch, *Anal. Chem.* **2005**, *77*, 5628.

[17] S. Yamamura, H. Kishi, Y. Tokimitsu, S. Kondo, R. Honda, S. R. Rao, M. Omori, E. Tamiya, A. Muraguchi, *Anal. Chem.* **2005**, *77*, 8050.

[18] J. Nilsson, M. Evander, B. Hammarstrom, T. Laurell, *Anal. Chim. Acta* **2009**, *649*, 141.

[19] J. Park, B. K. Lee, G. S. Jeong, J. K. Hyun, C. J. Lee, S. H. Lee, *Lab Chip* **2015**, *15*, 141.

[20] C. Stoecklin, Z. Yue, W. W. Chen, R. de Mets, E. Fong, V. Studer, V. Viasnoff, *Adv. Biosyst.* **2018**, *2*, 1700237.

[21] S. Yamamoto, J. Gaillard, B. Vianay, C. Guerin, M. Orhant-Prioux, L. Blanchoin, M. Thery, *EMBO J.* **2022**, *41*, 111631.

[22] B. Zheng, R. F. Ismagilov, *Angew. Chem. Int. Ed. Engl.* **2005**, *44*, 2520.

[23] W. A. Bauer, M. Fischlechner, C. Abell,W. T. Huck, *Lab Chip* **2010**, *10*, 1814.

[24] A. Gokaltun, Y. B. A. Kang, M. L. Yarmush, O. B. Usta, A. Asatekin, *Sci. Rep.* **2019**, *9*, 7377.

[25] N. Rousset, F. Monet, T. Gervais, *Sci. Rep.* **2017**, *7*, 245.

[26] L. Mathivet, S. Cribier, P. F. Devaux, *Biophys. J.* **1996**, *70*, 1112.

[27] M. I. Angelova, D. S. Dimitrov, *Faraday Discuss.* **1986**, *81*, 303.

[28] W. L. Haberman, R. M. Sayre, *David Taylor Model Basin Reports* **1958**, *1143*, 1.

[29] R. E. Waugh, *Biophys. J.* **1982**, *38*, 29.

[30] R. Dimova, C. Dietrich, A. Hadjiisky, K. Danov, B. Pouligny, *Eur. Phys. J. B* **1999**, *12*, 589.

[31] A. R. Honerkamp-Smith, F. G. Woodhouse, V. Kantsler, R. E. Goldstein, *Phys. Rev. Lett.* **2013**, *111*, 038103.

[32] Y. Sakuma, T. Kawakatsu, T. Taniguchi, M. Imai, *Biophys. J.* **2020**, *118*, 1576.

[33] H. A. Faizi, R. Dimova, P. M. Vlahovska, *Biophys. J.* **2022**, *121*, 910.

[34] Z. H. Huang, M. Abkarian, A. Viallat, *New J. Phys.* **2011**, *13*, 035026.

[35] Y. Shimizu, A. Inoue, Y. Tomari, T. Suzuki, T. Yokogawa, K. Nishikawa, T. Ueda, *Nat. Biotechnol.* **2001**, *19*, 751.

[36] Y. Shimizu, T. Kanamori, T. Ueda, *Methods* **2005**, *36*, 299.

[37] A. L. Marston, H. B. Thomaides, D. H. Edwards, M. E. Sharpe, J. Errington, *Gene Dev.* **1998**, *12*, 3419.

[38] I. Barak, K. Muchova, A. J. Wilkinson, P. J. O'Toole, N. Pavlendova, *Mol. Microbiol.* **2008**, *68*, 1315.

[39] N. Khalifat, N. Puff, S. Bonneau, J. B. Fournier, M. I. Angelova, *Biophys. J.* **2008**, *95*, 4924.

[40] Y. G. Liu, J. Agudo-Canalejo, A. Grafmuller, R. Dimova, R. Lipowsky, *ACS Nano* **2016**, *10*, 463.

[41] Z. T. Graber, Z. Shi, T. Baumgart, *Phys. Chem. Chem. Phys.* **2017**, *19*, 15285.

[42] I. Tsafrir, Y. Caspi,M. A. Guedeau-Boudeville, T. Arzi, J. Stavans, *Phys. Rev. Lett.* **2003**, *91*, 138102.

[43] J. Steinkuhler, P. De Tillieux, R. L. Knorr, R. Lipowsky, R. Dimova, *Sci. Rep.* **2018**, *8*, 11838.

[44] R. L. Knorr, H. Nakatogawa, Y. Ohsumi, R. Lipowsky, T. Baumgart, R. Dimova, *PLoS One* **2014**, *9*, e115357.

[45] J. C. Stachowiak, E. M. Schmid, C. J. Ryan, H. S. Ann, D. Y. Sasaki, M. B. Sherman, P. L. Geissler, D. A. Fletcher, C. C. Hayden, *Nat. Cell Biol.* **2012**, *14*, 944.

[46] B. Ramm, P. Glock, J. Mucksch, P. Blumhardt, D. A. Garcia-Soriano, M. Heymann, P. Schwille, *Nat. Commun.* **2018**, *9*, 3942.

[47] D. G. Gibson, L. Young, R. Y. Chuang, J. C. Venter, C. A. Hutchison 3rd, H. O. Smith, *Nat. Methods* **2009**, *6*, 343.

[48] Z. Petrasek, P. Schwille, *Biophys. J.* **2008**, *94*, 1437.

[49] L. He, B. Niemeyer, *Biotechnol. Prog.* **2003**, *19*, 544.

Figures

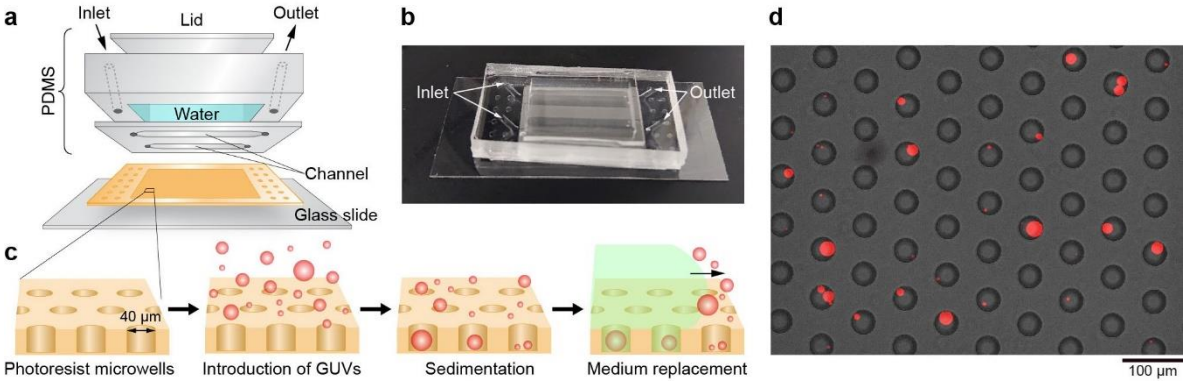

Figure 1. a) Schematic illustration of the microfluidic device composed of a microwell layer on a glass cover slide, and channel and water reservoir layers made of PDMS. b) Photograph of the device. The size of the glass cover slide is 24 mm × 50 mm. c) GUVs were introduced in the channels and settled in the microwells by sedimentation. The medium outside GUVs as replaced while the GUVs were trapped in the microwells. d) Merged picture of a fluorescence microscopy image of GUVs (red) and a phase-contrast image of 43 µm-deep microwells (grey). Separate images of each channel are shown in Figure S2 (Supporting Information).

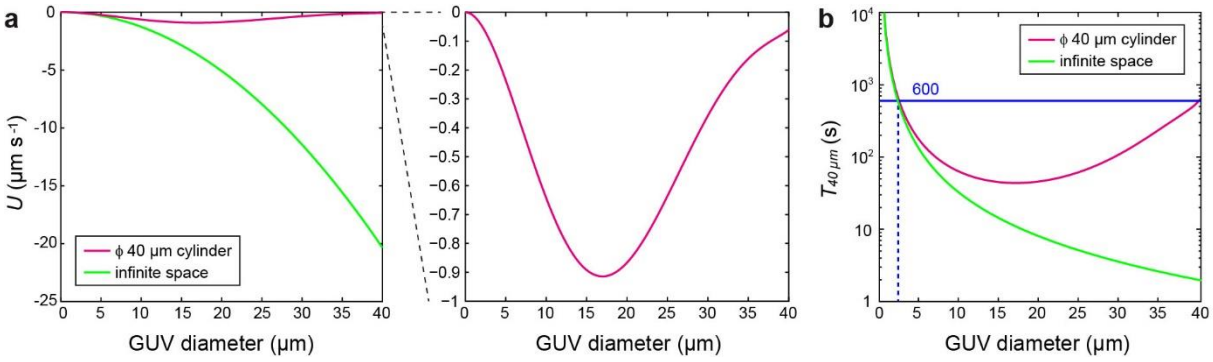

Figure 2. a) Terminal velocities *U* of a GUV sedimenting in a 40 µm-diameter cylinder magenta) and in an infinite medium (green) are plotted against GUV diameter. The right panel shows an enlarged view of the magenta curve. b) Times necessary for a GUV to sediment for a distance of 40 µm in a 40 µm-diameter cylinder (magenta) and in an infinite medium (green) are plotted against GUV diameter. Ten minutes (blue line) is enough for a majority of GUVs to sediment for 40 µm in the cylinder.

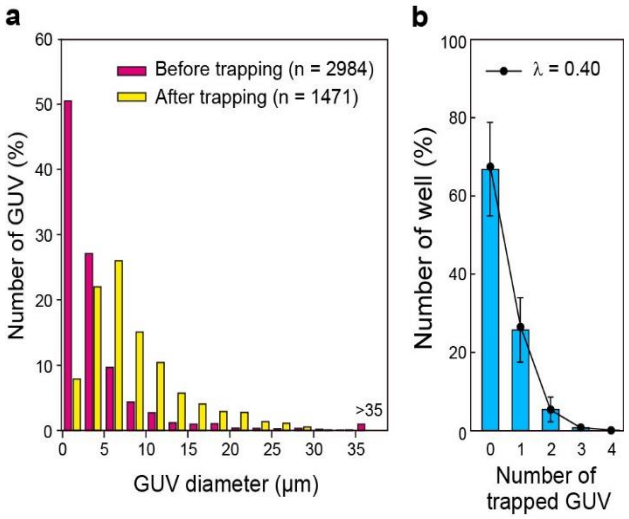

Figure 3. a) Size distribution of GUVs before (magenta) and after trapping (yellow). b) Percentage of microwells containing 0, 1, 2, 3, or 4 trapped GUVs averaged over 3 independent experiments (n = 3256, 6042, 5598 microwells). The black dots connected by a solid line represent the expected probability of trapping 0 to 4 GUVs given by the Poisson distribution with a mean number of GUV per well, $\lambda = 0.40 \pm 0.16$. Error bars represent standard deviation.

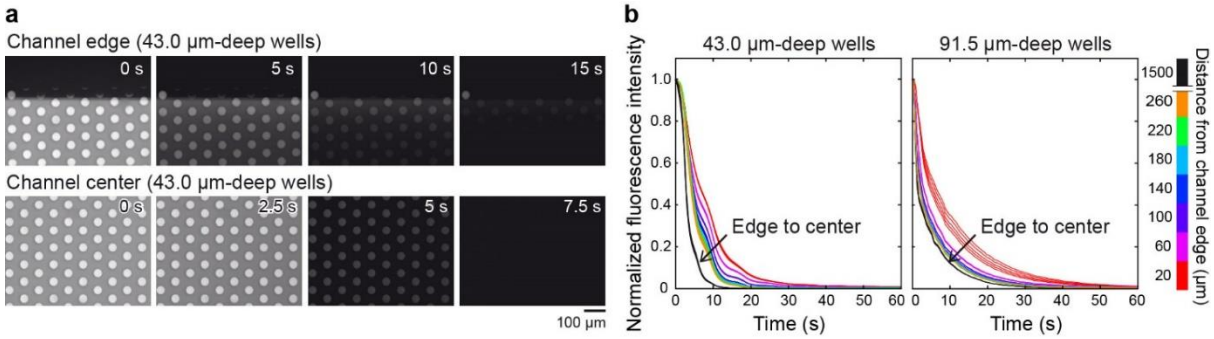

Figure 4. a) Fluorescence microscopy images of microwells at the edge of a channel (top) and at the center of the channel (bottom) at different time points underflow. The channel was initially filled with a fluorescein solution prior to the introduction at $t = 0$ of a non-fluorescent solution at a flow rate of ca. 0.90 µL s^{-1}. b) Fluorescence intensities normalized by maximum values at $t = 0$ in the microwell areas plotted against time. The distance between the microwell center and the channel edge is indicated by the color code on the right.

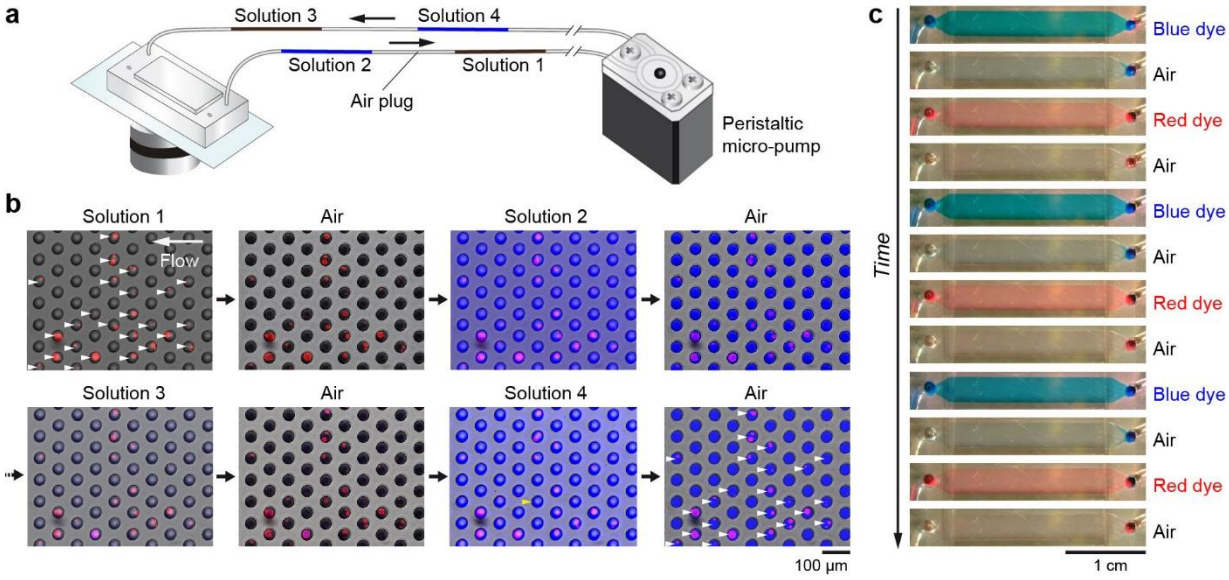

Figure 5. a) Scheme of the experimental setup. Non-fluorescent and fluorescent solutions, separated by air plugs, were introduced alternately into the microfluidic device containing GUVs by peristaltic micro-pump. b) Fluorescence microscopy images (GUV and fluorescein in red and blue, respectively) merged with phase-contrast microscopy images (grey) taken at different steps of the sequential medium exchanges using a microfluidic device with 91.5 µm-deep microwells. White arrowheads indicate the microwells containing GUVs before (top right) and after (bottom right) the medium exchanges, while a yellow arrowhead indicates a microwell where a GUV was lost during the operation. c) A series of images of an entire 46.3 µm-high channel, in which blue and red dyes separated by air plugs in a tubing were sequentially flowed by peristaltic micro-pump. Solutions were successfully exchanged without leaving air bubbles in the channel.

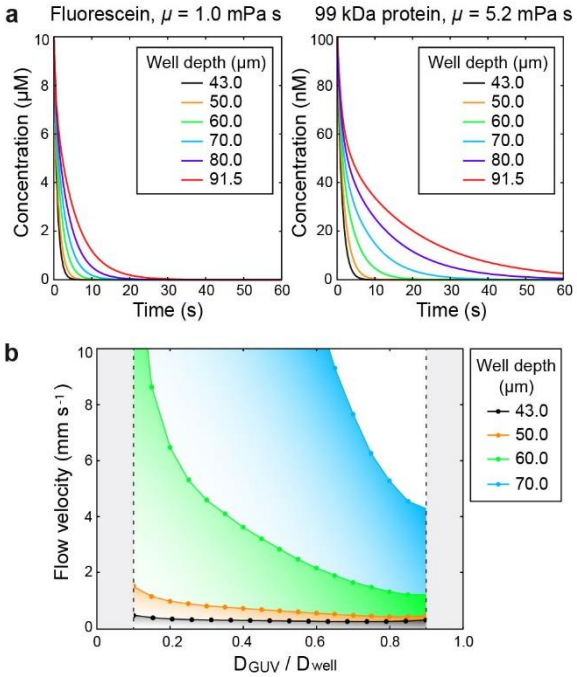

Figure 6. a) Molecular concentration change in a microwell with different depths under flow simulated by COMSOL. Results of fluorescein (diffusion coefficient $D = 4.3 \cdot 10^{-10}$ m^2 s^{-1}) in water (left) and 99 kDa protein ($D = 6.0 \cdot 10^{-11}$ m^2 s^{-1}) in a viscous medium (right), starting from an initial concentration of 10 μm and 100 nm, respectively. At $t > 0$, the same medium without fluorescein nor protein was introduced at the channel inlet at an average flow velocity fixed at 6.0 mm s^{-1}. The viscosity μ is indicated for each system. b) Phase diagram plotting the critical flow velocity at which the lift force equals the gravitational force on a GUV simulated by COMSOL against the relative GUV diameter compared to the microwell diameter (D_{GUV}/D_{well}, D_{well} = 40 μm) for different well depths. The viscosity of the medium was set as 1.0 mPa s.

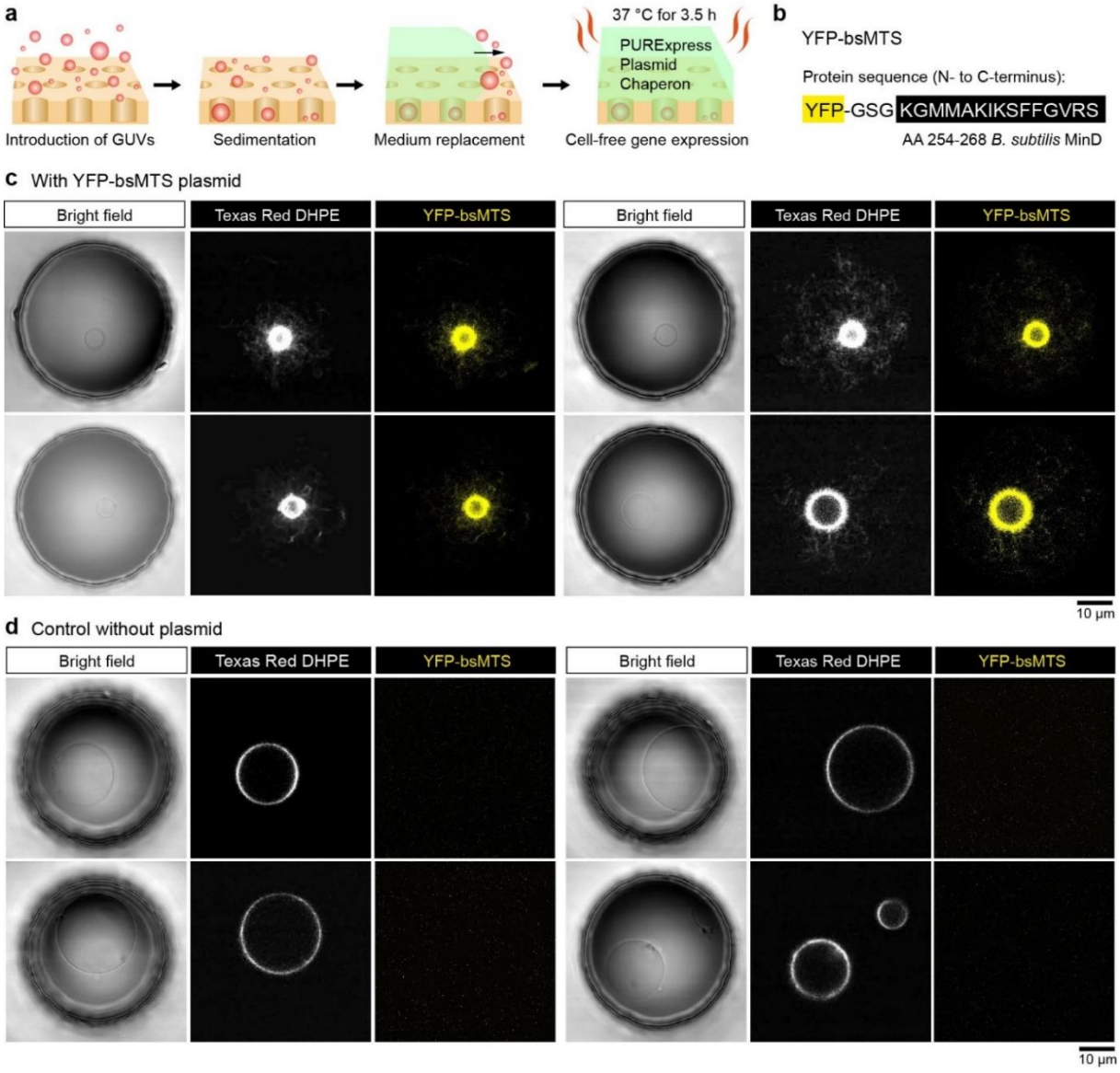

Figure 7. a) Scheme of the in situ cell-free gene expression in the presence of GUVs in the microfluidic device. b) Amino acid sequence of YFP-conjugated bsMTS coded on the plasmid DNA. c) Bright field images showing a microwell containing a GUV (gray), and confocal microscopy images of the GUV membrane (white), and YFP-bsMTS (yellow) after 3.5 h of gene expression at 37 °C. d) Results of the control experiment performed in the parallel channel on the same microfluidic device as c) without plasmid.

Supporting Information

Experimental

Materials and methods

Microfabrication of master molds. Chromium photomasks were designed on QCAD and CleWin5 software and printed by a micropattern generator (μPG 101, Heidelberg Instruments) on a mask blank (MB Whitaker & Associates). A negative photoresist dry film (50 μm-thick DF-1050 or 100 μm-thick DF-1100, Nagase ChemteX) was laminated on a 4-inch silicon wafer at 100 °C with a speed of 0.2 m min^{-1}. The wafer was cut into pieces with appropriate sizes after the lamination. A piece of the wafer was then exposed through a chromium photomask to 365 nm UV at 55.7 mW cm^{-2} by Lightning Cure LC8 (Hamamatsu Photonics) for 5 and 10 s for the 50 μm-thick and 100 μm-thick dry film, respectively. After a post-exposure bake at 100 °C for 10 min on a hotplate, the photoresist structure was developed with cyclohexanone (VWR Chemicals BDH), rinsed with ethanol, and dried under air flow. The obtained mold was annealed at 150 °C for 10 min on a hotplate and exposed to a vapor of trimethylchlorosilane (Sigma-Aldrich) for 5 min in a Petri dish at room temperature before the first use.

Fabrication of the microwells. Polydimethylsiloxane (PDMS) and its crosslinker (RTV 615, Momentive Performance Materials) were mixed at 10:1 ratio (w/w) and poured onto the master mold for the microwells, degassed, and allowed to reticulate at 75 °C for at least 4 h. The resulting PDMS block with an array of micro-pillars was then peeled off from the mold. Next, a drop of *ca.* 300 μL of OrmoStamp (Innodys) was deposited at the center of a glass cover slip (24 mm × 50 mm, 0.13-0.17 mm thickness) in an elongated shape. Subsequently, the micro-structured PDMS, which was kept under vacuum for 5 min immediately before use, was placed on the cover slip and pressed down with a 50 g cuboid weight for 10 min. Excess of OrmoStamp was wiped away with acetone (VWR International) prior to UV exposure on the sample at 21.6 mW cm^{-2} for 120 s from the cover slip side. Finally, the PDMS mold was carefully removed from the cover slip, leaving the OrmoStamp microwells on it.

Fabrication of the channels and the water reservoir. *Ca.* 1 mm- or 2 mm-thick layer of the mixture of PDMS and crosslinker (10:1 w/w) was deposited on the master mold for the channels, degassed, and heated at 100 °C on a hotplate for 10 min. The PDMS layer

was then cut, peeled off and laid down on a glass slide with the channel side down. The 2 mm-thick channel layer was used specifically for the air-plug experiments. A 40 mm × 19 mm rectangular PDMS block with a 19 mm × 11 mm rectangular hole was cut out from a 5 mm-thick PDMS sheet by a scalpel and bound on the channel layer immediately after a plasma treatment on the both surfaces (air plasma, Harrick PDC-002 equipped with a PDC-FMG PlasmaFlo). 1 mm- or 1.5 mm diameter holes were made at the inlets and outlets of the channels by a biopsy punch (Kai Medical) and thoroughly rinsed with ethanol.

For the experiment with air plugs, to make the PDMS surface hydrophilic, 0.25% (w/w) of PDMS-EtO (Gelest, Inc.) was added to the PDMS mixture for both the channels and the reservoir, and instead of air plasma, an oxygen plasma treatment was carried out for the bonding at 30 W for 1 min under 8 sccm oxygen flow and 0.15 Torr vacuum (CUTE, Femto Science). The PDMS-EtO concentration in PDMS was selected to achieve a balance between optical transparency, bonding efficiency, and hydrophilicity of the solidified PDMS/PDMS-EtO mixture. The parameters of the oxygen plasma treatment were also optimized for ensuring reliable bonding between 2 layers of PDMS/PDMS-EtO, and between PDMS/PDMS-EtO and the microwell substrate.).

A piece of *ca.* 1 mm-thick PDMS sheet was prepared as a lid to cover the rectangular hole, which served as a water reservoir.

Microfluidic device assembly. The surfaces of the microwell substrate and the PDMS block with the channels were activated by plasma treatment (air plasma for normal PDMS and oxygen plasma for PDMS/PDMS-EtO, respectively) and covalently bonded. To avoid the adhesion of lipid bilayer membranes or proteins on the microwell and channel surfaces, 15 μL of 0.5% (w/v) β-casein or 5% (w/v) bovine serum albumin (BSA) in phosphate-buffered saline (PBS) (Sigma-Aldrich) was injected into each channel by micropipette immediately after the plasma bonding. The BSA-treated device was specifically used for the cell-free gene expression experiments. The reservoir above the channels was then filled with water and closed with the lid. The whole device was sealed in a Petri dish with a wet tissue and kept overnight at room temperature before use.

GUV preparation. L-α-phosphatidylcholine from chicken egg (EPC), 1,2-dioleoyl-sn-glycero-3-phosphocholine (DOPC), and 1,2-dioleoyl-sn-glycero-3-phospho-(1'-rac-glycerol) (DOPG) were obtained from Avanti Polar Lipids. Texas Red 1,2-dihexadecanoyl-sn-glycero-3-phosphoethanolamine (Texas Red DHPE) was purchased from Thermo Fisher Scientific. GUVs were prepared by electro-formation method as follows.[1-2] Either EPC or a 4:1 (mol/mol) mixture of DOPC and DOPG was dissolved in chloroform at a concentration of 0.5 mg mL^{-1}, together with Texas Red DHPE at 2.5 μg mL^{-1}. Twenty μL of the lipid mixture was spread onto the conductive surfaces of two indium tin oxide-coated glass slides (ITO slides, Präzisions Glas & Optik) by micropipette, covering an area of *ca.* 1.5 cm × 2 cm. The obtained lipid films on ITO slides were protected from light and further dried under vacuum for 2 h at room temperature. Sucrose solution (see below) was then sealed between the lipid-deposited surfaces of ITO slides by using a 2 mm-thick PDMS spacer. Immediately after sealing, 2 V peak-to-peak AC voltage at 10 Hz was applied between the ITO slides for 4 h at room temperature to form GUVs while the sample was protected from light. The GUV solution was collected in a microcentrifuge tube, kept at 4 °C, and used within 2 days. Sucrose and D-(+)-glucose were separately dissolved in MilliQ water at an osmolality of 300 mOsm or 1.72 Osm adjusted by osmometer (Type 15, Löser Messtechnik). After the electro-formation of GUVs in a sucrose solution, the GUV solution was mixed with a glucose solution with the same osmolality as the sucrose solution at 1:1 (v/v) ratio. GUVs were introduced in the microfluidic device, which was rinsed 3 times with 20 μL of the glucose solution in advance.

Fluid manipulation. Fluids were introduced into the microfluidic device either manually by micropipette, or by a finger-sized micro-peristaltic pump (RP-TX, Takasago Fluidic Systems) equipped with a motor controller (RE-C100, Aquatech) and connected to the device via polytetrafluoroethylene tubing with an inner and an outer diameter of 0.56 and 1.07 mm, respectively (Adtech Polymer Engineering). Fluids were visualized, when necessary, with 10 μM fluorescein (Sigma-Aldrich) in PBS or with food coloring (Vahiné) 5 times diluted in PBS.

Plasmid construction and Cell-free expression of PhiYFP-bsMTS. The membrane-targeting sequence (MTS) of *B. subtilis* MinD, bsMTS[3], was fused to the yellow fluorescent protein PhiYFP by Gibson isothermal assembly[4] of two gene fragments

obtained by PCR amplification (Q5 HF-hot start, NEB) of a PhiYFP expression plasmid under a T7 promoter with primers overlapping in the middle of the bsMTS coding sequence (bsMTS: AAAGGTATGATGGCTAAAATCAAATCTTTCTTCGGTGTTC GTTCT). The plasmid was further amplified using NEB 5-α competent *E. coli* and purified with Monarch Miniprep kit (NEB). The constructed PhiYFP-bsMTS T7-expression plasmids were expressed *in vitro* using PURExpress protein synthesis system (NEB). Ten µL of PURExpress solution A, 7.5 µL of PURExpress solution B, 1 µL i.e., 40 U of murine RNase inhibitor (NEB), 1 µL each of DnaK Mix (100 µM DnaK, 20 µM DnaJ, 20 µM GrpE), 60 mM GSSG, and 320 µM DsbC (GeneFrontier Corporation) were mixed in a microcentrifuge tube on ice. Then, 10.74 µL each of the mixture was added to 2 microcentrifuge tubes containing 1.75 µL of Nuclease-free water (Thermo) with or without the plasmid DNA at a final concentration of 4 ng μL^{-1}. Ten µL each of those solutions was introduced in each channel of the microfluidic device after GUV sedimentation.

Microscopies and profilometer. Images were taken by an epifluorescence microscopy (Axio Observer Z1, Zeiss) equipped with an electron-multiplying CCD camera C11440 (Hamamatsu Photonics) through a N-Achroplan 5× (NA 0.15) or 10× (0.25) objective (Zeiss), by a confocal microscopy (LSM 900, Zeiss) via a Plan-Apochromat 40× (NA 1.4) oil immersion objective (Zeiss), and by a Dino-Lite handheld digital microscope (AnMo Electronics Corporation). The height of the microstructures was measured using an optical profilometer, Wyko NT9100 (Veeco).

Viscosity measurements. A rheometer MCR302 (Anton Paar) was used to measure the viscosities of the sugar solutions at room temperature.

COMSOL simulations. Numerical simulations were conducted using COMSOL Multiphysics v.6.0 software. For simplicity, the model geometry built in 3D consisted of a 400 µm-long, 300 µm-wide, and 46.3 µm-high cuboidal channel with 9 wells at the channel bottom with a diameter of 40 µm, a depth of h µm, and an interval of 40 µm as illustrated in Figure S4. A solid sphere with a radius of r µm as a model of GUV was placed in one of the microwell, keeping a distance of 1 µm from the well walls on the upstream side and at the bottom. The simulations were conducted by coupling together the modules of Lamina Flow and Transport of Diluted Species. No-slip condition was

introduced at the walls. Symmetry features and user-defined mesh size were employed. Only finer meshing was applied to the sphere and its microwell.

To compute the diffusion of molecules under flow condition, and to be consistent with the experimental conditions used, the whole geometry was assumed initially (at $t = 0$) filled with either 10 µM fluorescein (diffusion coefficient $D = 4.3 \cdot 10^{-10}$ m^2 s^{-1})[5] or 100 nM of 99 kDa protein ($D = 6.0 \cdot 10^{-11}$ m^2 s^{-1})[6] in a medium of 1.0 mPa s or 5.2 mPa s viscosity, respectively. At $t > 0$, the same medium without fluorescein nor protein was introduced at the entrance of the channel at a mean velocity of 6.0 mm s^{-1} with no stress (0 Pa) applied at the outlet. The average concentrations of fluorescein and protein in the microwells were evaluated from concentration profiles simulated at different times and for different well depths (h = 43, 50, 60, 70, 80, and 91.5 µm). Since no significant difference between the 9 microwells was observed, only the values obtained at the microwell closest to the inlet were considered plotted in Figure 6a.

To simulate the net forces acting on a GUV, *i.e.*, a sphere at the bottom of the well, lift force F_{lift} was computed using the *reacf* operator integrated into COMSOL as described by Rousset, *et al*.[7] First, we successfully verified that our simulations reproduced the same results as in reference[7] with identical set of parameters. Secondly, critical flow velocities, at which the lift force F_{lift} equals the gravitational force F_g ($\boldsymbol{F_g = 4\pi r^3 g(\rho_i - \rho_o)/3}$), were evaluated by sweeping flow velocity for several sets of well depth h and GUV size ($D_{GUV} = 2r$), the well diameter being fixed at D_{well} = 40 µm. Indeed, to retain the GUV inside a microwell, the gravitational force F_g has to surpass F_{lift}, when ρ_i is equal to $1.037 \cdot 10^3$ kg m^{-3} (300 mOsm sucrose solution) and ρ_o is equal to $1.0 \cdot 10^3$ kg m^{-3} (PBS). As a result, the critical flow velocities were plotted against the size ratio D_{GUV}/D_{well} in order to build the phase diagram shown in Figure 6b.

Figures

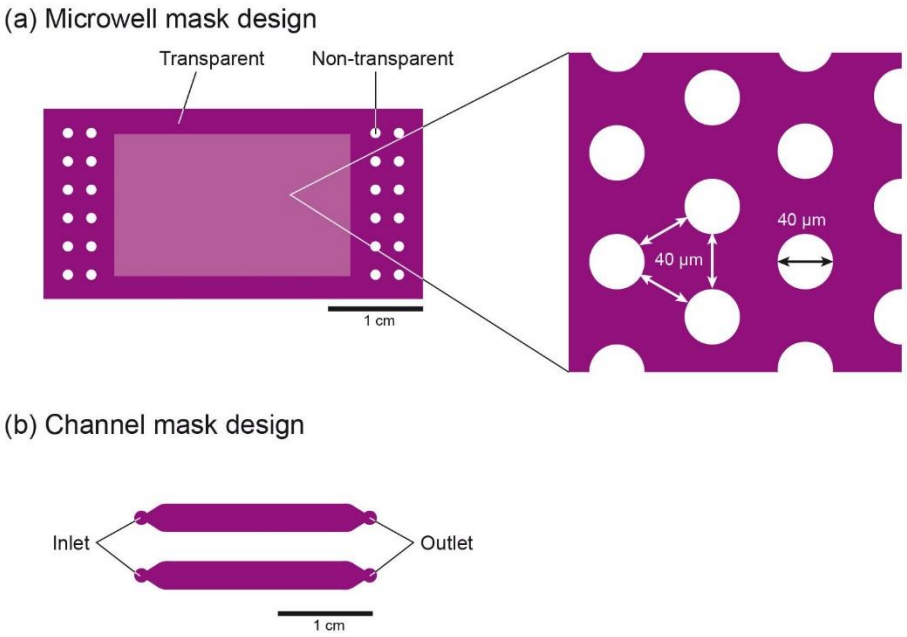

Figure S1 (a) Mask design for photolithography with a negative photoresist dry film to fabricate the microwell mold. (b) Mask design for the mold of two parallel channels.

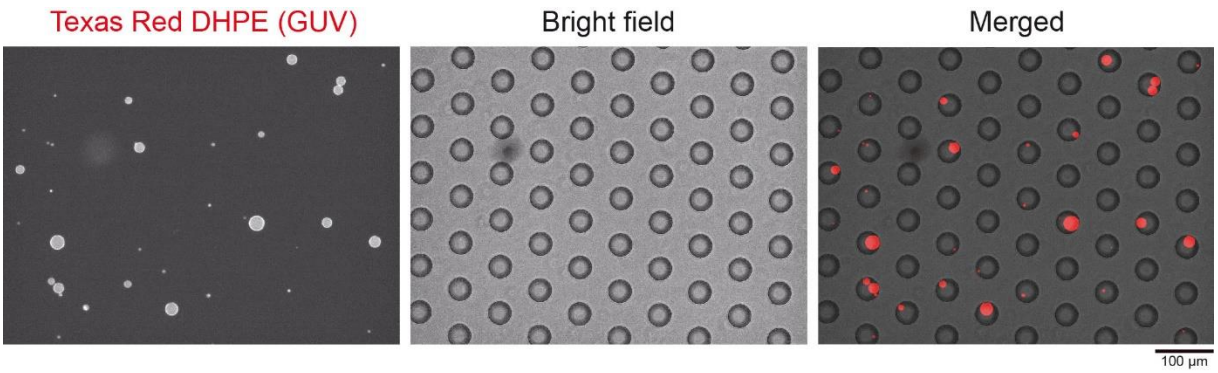

Figure S2 Fluorescence microscopy image of GUVs (left), phase-contrast image of 43 µm-deep microwells (center), and their merged image (right) corresponding to Figure 1d.

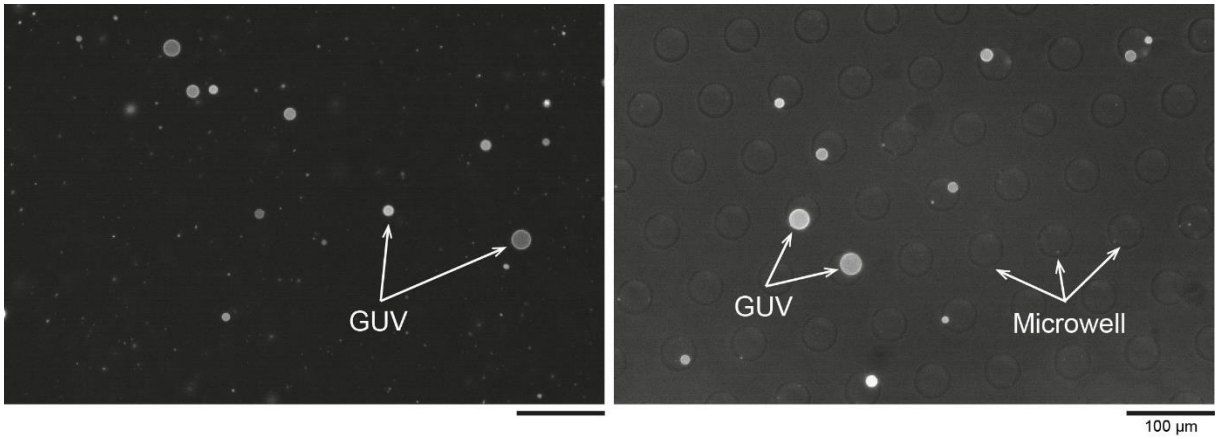

Figure S3 Fluorescence microscopy image of an initial GUV solution, i.e., 1:1 (v/v) mixture of a sucrose solution containing GUVs and a glucose solution at a same osmolarity, introduced in a 46.3 µm-high channel without microwell (left). The image was taken 10 min after the introduction, so that GUVs not smaller than 3 µm sediment at the channel bottom. A merged image of fluorescence and phase-contrast microscopy after GUV trapping using the same GUV solution (right).

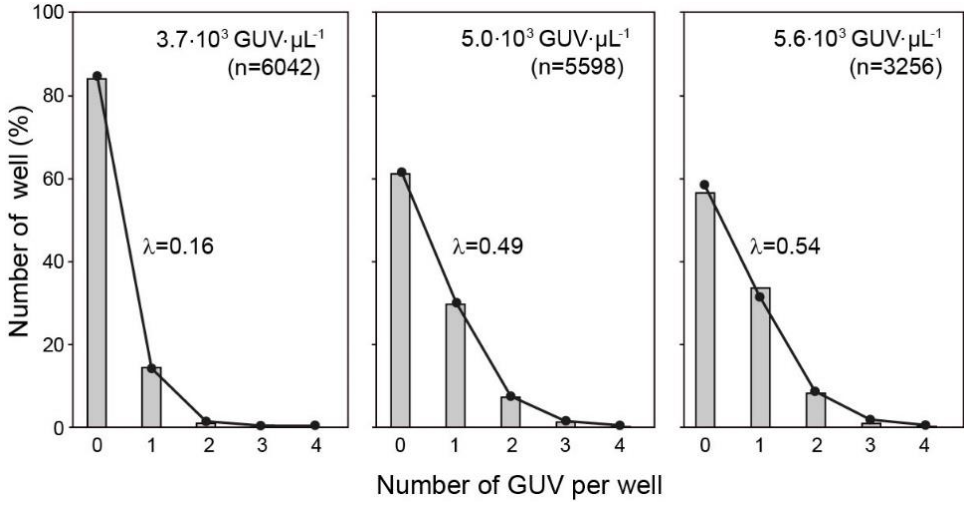

Figure S4 Percentage of microwells containing 0, 1, 2, 3 or 4 trapped GUVs from 3 independent experiments with different initial GUV densities, which are indicated in each graph, along with the number of microwells counted, n. The black dots connected by a solid line represent the expected probability of trapping 0 to 4 GUVs given by the Poisson distribution with a mean number of GUV per well, λ. GUVs smaller than 3 µm were eliminated from the analyses.

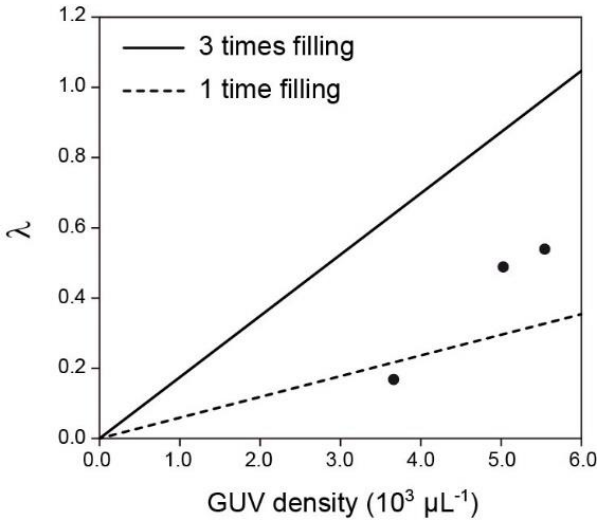

Figure S5 Mean number of GUV per microwell, λ, plotted against the initial GUV density. The filled circles represent the experimental data we obtained from 3 independent experiments, while the solid line represents the theoretical λ_{theo}, which was calculated as $\boldsymbol{\lambda_{theo} = 3\delta_{GUV} \cdot H \cdot \pi R^2}$, where δ_{GUV}, H, R are the GUV density, channel height, and microwell radius, respectively. The factor 3 originates from the fact that we introduced GUV solution 3 times in the channel to increase the number of GUVs trapped in microwells. The dashed line for a comparison represents the theoretical λ when GUVs are introduced only once in the channel.

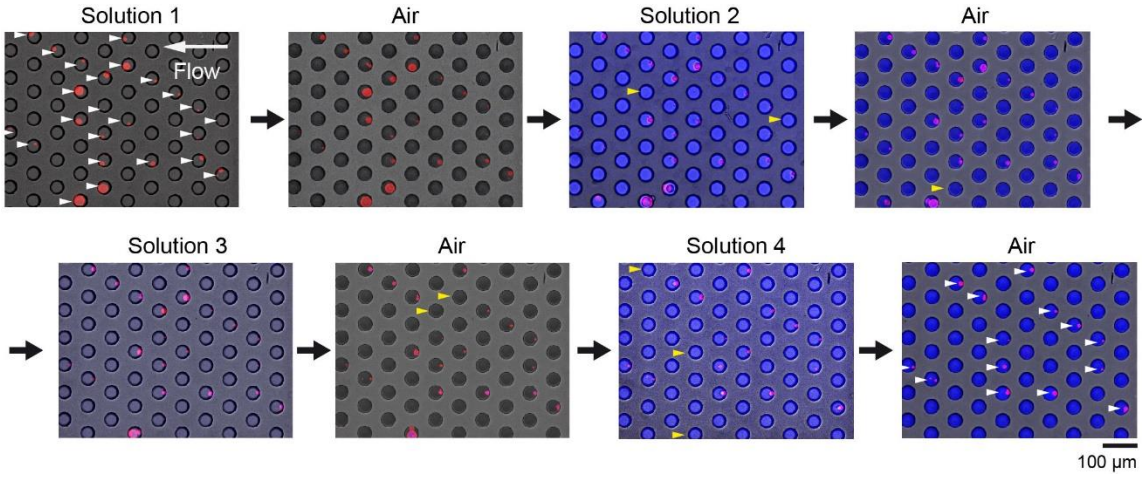

Figure S6 Fluorescence microscopy images (GUV and fluorescein in red and blue, respectively) merged with phase-contrast microscopy images (grey) taken at different steps of sequential medium exchanges using a microfluidic device with 43.0 µm-deep microwells. White arrowheads indicate the microwells containing GUVs before and after the medium exchanges, while yellow arrowheads indicate microwells where a GUV was lost during the operation.

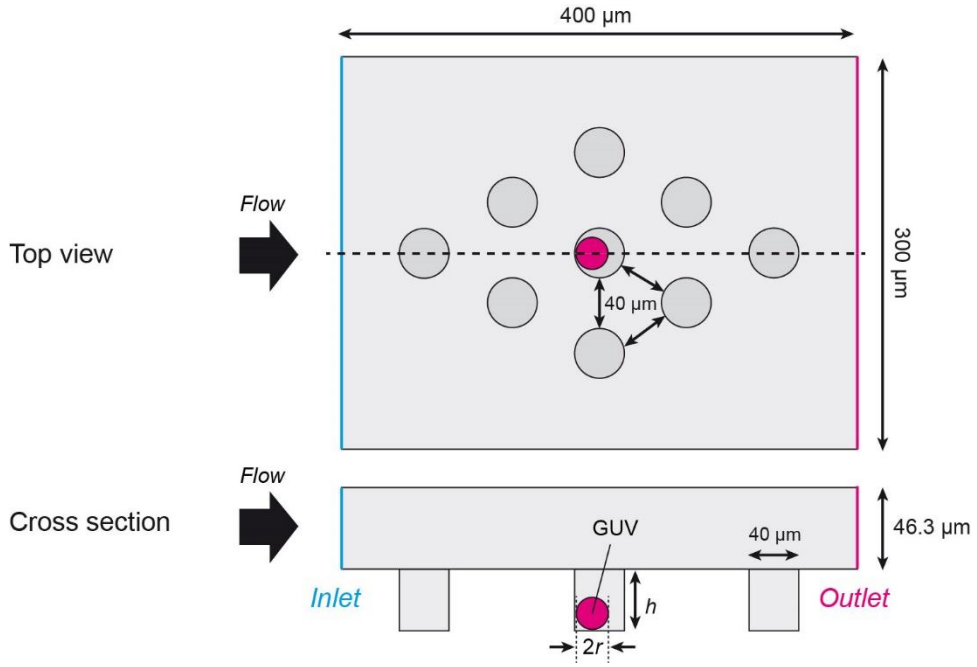

Figure S7 3D geometry used for the COMSOL simulations.

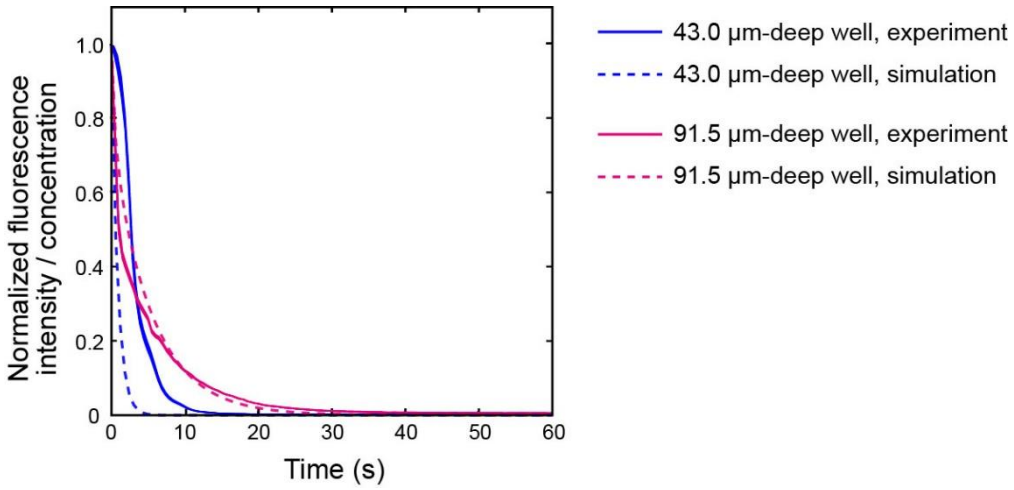

Figure S8 Comparison between the experimental data (solid lines) and simulation results (dashed lines) on fluorescein diffusion from 43.0 μm-deep (blue) and 91.5 μm-deep (magenta) microwells at the widthwise center of the channel.

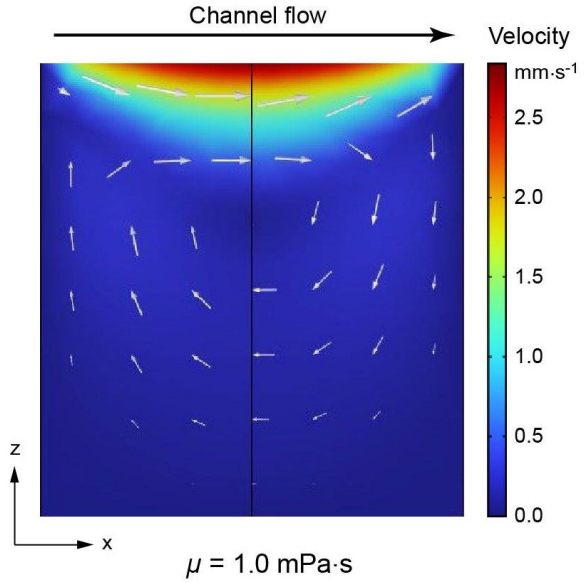

Figure S9 Cross-sectional view of the flow velocity profile at the center of a 40 μm-diameter 43 μm-deep microwell simulated by COMSOL. The velocities at different positions are indicated with the color code shown on the right, as well as with the white arrows, whose lengths and directions correspond to the logarithm of the velocity and the flow direction, respectively. The direction of the flow in the channel above is indicated with a black arrow at the top of the image. The viscosity was set as 1.0 mPa s in this simulation, and no significant difference was observed when the viscosity was set as 5.2 mPa s.

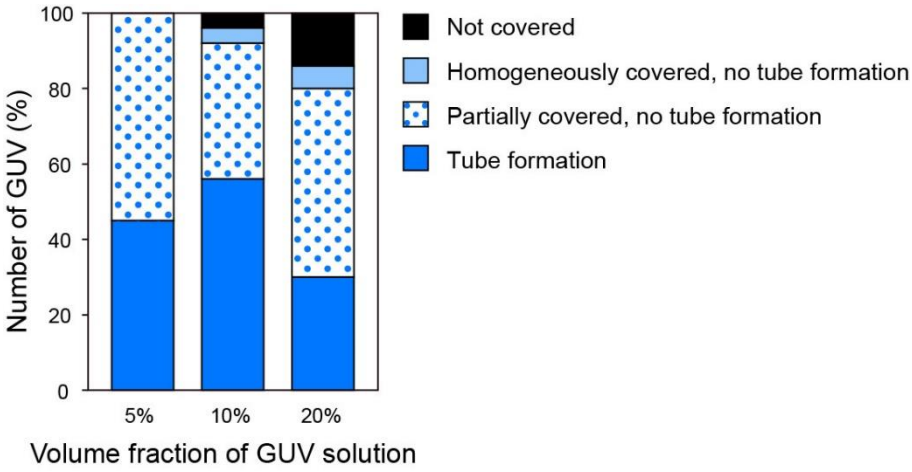

Figure S10 Cell-free expression of YFP-bsMTS in the presence of GUVs. Five, 10, or 20% volume fraction of a sucrose solution containing GUVs was added to the cell-free gene expression medium, mixed in a 0.2 mL microtube by 20 times tapping, and incubated at 37 °C for 3.5 h. The final volume of each mixture was 10 µL. The samples were transferred in 3 mm-diameter observation chambers made of PDMS and a glass cover slip, and observed by confocal microscopy. The chambers were treated with 5% (w/v) BSA in PBS for 1 h at room temperature and rinsed with 1.72 Osm glucose solution immediately before use. Membrane tube formation was observed on 45, 56, and 30% of GUVs (blue), while 55, 36, and 50% of GUVs were partially covered with the protein showing bright spots on GUVs (blue dots), 0, 4, 6% of GUVs were homogeneously covered by the protein without tube formation (light blue), and no protein binding was observed on 0, 4, 14% of GUVs (black), for the samples containing 5, 10, 20% (v/v) GUV solution, respectively (n = 51, 25, 64).

References

[1] L. Mathivet, S. Cribier, P. F. Devaux, *Biophys. J.* **1996**, *70*, 1112.
[2] M. I. Angelova, D. S. Dimitrov, *Faraday Discussions* **1986**, *81*, 303.
[3] B. Ramm, P. Glock, J. Mucksch, P. Blumhardt, D. A. Garcia-Soriano, M. Heymann, P. Schwille, *Nat. Commun.* **2018**, *9*, 3942.
[4] D.G. Gibson, L. Young, R.-Y. Chuang, J. C. Venter, C. A. Hutchison, H. O. Smith, *Nat. Methods* **2009**, *6* (5), 343.
[5] Z. Petrasek, P. Schwille, *Biophys. J.* **2008**, *94*, 1437.
[6] L. He, B. Niemeyer, *Biotechnol. Prog.* **2003**, *19*, 544.
[7] N. Rousset, F. Monet, T. Gervais, *Sci Rep* **2017**, *7*, 245.